Density Functional Study of the Mechanism of the Palladium(II)-Catalyzed Ethylene Polymerization Reaction

Djamaladdin G. Musaev, Mats Svensson, and Keiji Morokuma*

Cherry L. Emerson Center for Scientific Computation and Department of Chemistry, Emory University, Atlanta, Georgia 30322

Staffan Strömberg and Krister Zetterberg

Department of Chemistry, Organic Chemistry at the Royal Institute of Technology, S-100 44 Stockholm, Sweden

Per E. M. Siegbahn

Department of Physics, Stockholm University, Box 6730, S-113 85 Stockholm, Sweden

Received December 9, 1996[⊗]

The hybrid density functional B3LYP method has been used to study the mechanism of ethylene polymerization catalyzed by the Pd(II) diimine complex. The chain initiation starts with coordination of ethylene to the active catalyst $[L_2PdCH_3]^+$, followed by ethylene migratory insertion into the Pd−alkyl bond to form a γ-agostic intermediate, which rearranges to a more stable β-agostic form. The chain propagation starting with the β-agostic complex **7** can proceed via pathway **A** through coordination, migratory insertion, and rearrangement, leading to linear polyethylene, or pathway **B**, through β-hydride elimination, olefin rotation, and reinsertion to give a branched alkyl intermediate, which can then coordinate ethylene and produce branched polyethylene. The rate-determining step is olefin insertion, and the olefin alkyl complexes are the resting states in the catalytic cycle. Associative displacement, where the coordinated polymer is associatively replaced from the same diimine−Pd−hydrido−olefin complex **7** by ethylene in solution, is likely to be a preferable chain transfer pathway.

Introduction

Transition-metal-catalyzed olefin polymerization reactions and their mechanisms have been subject to extensive experimental[1] and theoretical[2] studies with the goal of better control of polymer microstructures and molecular weights and discovery of new and more efficient catalysts. Metallocenes and geometry-constrained catalysts of the d^0 and d^0f^n elements have been the main focus of such studies. However, different complexes such as diimine−M(II) (M = Ni, Pd)[3] and chelating alkoxide−M(IV) (M = Ti, Zr)[2b,4] complexes have recently been reported to catalyze ethylene polymerization. The mechanism of these new catalytic processes and its differences from and similarities with the widely used metallocene-based process is of great interest from both fundamental and practical points of view. In a previous paper[5] we have studied the mechanism of the diimine−Ni(II)-catalyzed ethylene polymerization using the density functional theory. The present paper is a similar study of the diimine−Pd(II)-catalyzed process, the goal of which is to study the following elementary reactions

chain initiation (olefin coordination and insertion):

$$[L_2MCH_3]^+ + C_2H_4 \rightarrow [L_2MCH_2CH_2CH_3]^+ \quad (1)$$

chain propagation (olefin coordination and insertion giving a linear polymer):

$$[L_2MCH_2CH_2CH_3]^+ + C_2H_4 \rightarrow [L_2M(CH_2CH_2)_2CH_3]^+ \quad (2)$$

[⊗] Abstract published in *Advance ACS Abstracts,* April 1, 1997.

(1) As leading references, see: (a) Coates, G. W.; Waymouth, R. M. *Science* **1995**, *267*, 217. (b) van der Linden, A.; Schaverien, C. J.; Meijboom, N.; Ganter, C.; Orpen, A. G. *J. Am. Chem. Soc.* **1995**, *117*, 3008. (c) Yang, X.; Stern, C. L.; Marks, T. J. *J. Am. Chem. Soc.* **1994**, *116*, 10015. (d) Coughlin, E. B.; Bercaw, J. E. *J. Am. Chem. Soc.* **1992**, *114*, 7606. (e) Crowther, D. J.; Baenziger, N. C.; Jordan, R. F. *J. Am. Chem. Soc.* **1991**, *113*, 1455. (f) Kaminsky, W.; Kulper, K.; Brintzinger, H. H.; Wild, F. R. W. P. *Angew. Chem., Int. Ed. Engl.* **1985**, *24*, 507. (g) Ewen, J. A. *J. Am. Chem. Soc.* **1984**, *106*, 6355.

(2) For leading references, see: (a) Yoshida, T.; Koga, N.; Morokuma, K. *Organometallics* **1995**, *14*, 746. (b) Yoshida, T.; Koga, N.; Morokuma, K. *Organometallics* **1996**, *15*, 766. (c) Woo, T. K.; Fan, L.; Ziegler, T. *Organometallics* **1994**, *13*, 2252. (d) Fan, L.; Harrison, D.; Woo, T. K.; Ziegler, T. *Organometallics* **1995**, *14*, 2018. (e) Hyla-Kryspin, I.; Niu, S.; Gleiter, R. *Organometallics* **1995**, *14*, 964.

(3) Johnson, L. K.; Killian, C. M.; Brookhart, M. *J. Am. Chem. Soc.* **1995**, *117*, 6414.

(4) Froese, R. D. J.; Musaev, D. G.; Matsubara, T.; Morokuma, K. Submitted for publication.

(5) Musaev, D. G.; Froese, R. D. J.; Svensson, M.; Morokuma, K. *J. Am. Chem. Soc.* **1997**, *119*, 367.

S0276-7333(96)01033-3 CCC: $14.00

chain propagation (β-hydride elimination and olefin reinsertion giving a branched polymer):

$$[L_2MCH_2CH_2CH_3]^+ \rightarrow [L_2M(H)(CH_2{=}CHCH_3)]^+ \rightarrow [L_2MCH(CH_3)_2]^+ + C_2H_4 \rightarrow [L_2MCH_2CH_2CH(CH_3)_2]^+ \quad (3)$$

chain termination or chain transfer (β-hydride elimination and olefin dissociation):

$$[L_2MCH_2CH_2CH_3]^+ \rightarrow [L_2M(H)(CH_2{=}CHCH_3)]^+ \rightarrow [L_2MH]^+ + CH_2CHCH_3 \quad (4)$$

chain termination or chain transfer (hydrogenolysis):

$$[L_2MCH_2CH_2CH_3]^+ + H_2 \rightarrow [L_2M(H_2)CH_2CH_2CH_3]^+ \rightarrow [L_2MH]^+ + CH_3CH_2CH_3 \quad (5)$$

for the M = Pd and L_2 = HN=C(H)C(H)=NH, in order to answer the following questions.

(i) What are the structures and relative energies of the reactants, intermediates, transition states and products of the reactions (1)−(5)?

(ii) What is the rate-determining step of the entire diimine−Pd(II)-catalyzed ethylene polymerization process?

(iii) What is the chain termination step of the reaction, and how can the weight of the polymers be controlled?

(iv) What are factors controlling the structure of the polyethylenes?

We plan to compare systematically the mechanisms of the diimine−Ni(II)-, diimine−Pd(II)-, and metallocene-catalyzed ethylene polymerization reactions in a separate paper due to their extreme importance.

Calculation Procedure

Geometries and energies of the reactants, intermediates, transition states, and products of the reactions (1)−(5) are calculated using the hybrid density functional B3LYP method,[6] which has been shown to predict quite reliable geometries and energetics.[7] In these calculations we mainly used two basis sets. Basis set I (below denoted as BSI), used for geometry optimization, includes a double ζ-valence basis set, {5s5p4d}/[3s3p2d], for Pd with the relativistic ECP by Hay and Wadt[8] replacing core electrons up to 3d and a double-ζ quality basis set of Huzinaga and Dunning[9] for the active part, i.e. C and H atoms of alkyl groups and olefins, while the standard 3-21G basis set[10] was adopted for N, C, and H atoms of the inert HN=C(H)C(H)=NH ligand. The relative energies are not significantly affected by the choice of the less accurate 3-21G set for this part of the metal complexes in the geometry optimizations. Basis set II (below denoted as BSII) was used for recalculation of the energetics at the B3LYP/BSI optimized geometries. For the Pd atom it has the same primitive basis set as BSI, but the 5s, 5p, and 4d shells have a triple-ζ valence contraction and a polarization f function.[11] For olefins and alkyl groups, polarization d_C (α = 0.75) and p_H (α = 1.0) functions were added to the BSI. Also, BSII uses the Huzinaga−Dunning[9] double-ζ basis set for carbon, nitrogen, and hydrogen of the inert ligand L. Below, we will discuss the energetics obtained only with BSII. All structures were optimized without symmetry constraints. Normal mode analysis, zero-point energy correction (ZPC), and Gibbs free energy calculations have been done for the reactants, intermediates, transition states, and products of the chain initiation reaction (1) using BSI. We assumed that the values of the zero-point, thermal, and entropy corrections will not change upon going from BSI to BSII and simply added their values calculated using BSI to the energetics obtained using BSII. The Gibbs free energy was calculated at 298 K and 1 atm. All calculations have been performed with the Gaussian-94 package,[12] supplemented by our own ECP analytical second-derivative code.[13]

Results and Discussion

The calculated geometries of the reactants, intermediates, transition states, and products of the reactions (1)−(5) are illustrated in Figures 1−6. Their relative energies are given in Table 1, and in Figure 7 the potential energy profile (PEP) of the reactions (1)−(5) is presented. In Table 2, the binding energies of important bonds of the products and intermediates of the reactions (1)−(5) are given.

A. Chain Initiation. We will begin our discussions with reaction 1. As proposed by Brookhart and coworkers,[3] the active reactant of reaction 1 is the complex **1**, which, positively characterized as being a real minimum, has a planar structure with Pd−N^1 and Pd−N^2 bond lengths of 2.01 and 2.20 Å. This difference in the Pd−N bond lengths is a result of the *trans* influence from the CH_3 group on the Pd−N^2 bond. The Pd−C−H^1 angle is found to be about 10° smaller than the Pd−C−H^2 and Pd−C−H^3 angles. It is difficult to prove the existence of a Pd···H^1 agostic interaction in structure **1**. In solution, this coordinatively unsaturated intermediate is likely to be solvated by a solvent molecule in the first shell.

(6) (a) Becke, A. D. *Phys. Rev. A* **1988**, *38*, 3098. (b) Lee, C.; Yang, W.; Parr, R. G. *Phys. Rev. B* **1988**, *37*, 785. (c) Becke, A. D. *J. Chem. Phys.* **1993**, *98*, 5648.

(7) . (a) Musaev, D. G.; Morokuma, K. *J. Phys. Chem.* **1996**, *100*, 6509. (b) Erikson, L. A.; Pettersson, L. G. M.; Siegbahn, P. E. M.; Wahlgren, U. *J. Chem. Phys.* **1995**, *102*, 872. (c) Ricca, A.; Bauschlicher, C. W., Jr. *J. Phys. Chem.* **1994**, *98*, 12899. (d) Heinemann, C.; Hertwig, R. H.; Wesendrup, R.; Koch, W.; Schwarz, H. *J. Am. Chem. Soc.* **1995**, *117*, 495. (e) Hertwig, R. H.; Hrusak, J.; Schroder, D.; Koch, W.; Schwarz, H. *Chem. Phys. Lett.* **1995**, *236*, 194. (f) Schroder, D.; Hrusak, J.; Hertwig, R. H.; Koch, W.; Schwerdtfeger, P.; Schwarz, H. *Organometallics* **1995**, *14*, 312. (g) Fiedler, A.; Schroder, D.; Shaik, S.; Schwarz, H. *J. Am. Chem. Soc.* **1994**, *116*, 10734. (h) Fan, L.; Ziegler, T. *J. Chem. Phys.* **1991**, *95*, 7401. (i) Berces, A.; Ziegler, T.; Fan, L. *J. Phys. Chem.* **1994**, *98*, 1584. (j) Lyne, P. D.; Mingos, D. M. P.; Ziegler, T.; Downs, A. J. *Inorg. Chem.* **1993**, *32*, 4785. (k) Li, J.; Schreckenbach, G.; Ziegler, T. *J. Am. Chem. Soc.* **1995**, *117*, 486.

(8) (a) Hay, P. J.; Wadt, W. R. *J. Chem. Phys.* **1985**, *82*, 299. (b) Wadt, W. R.; Hay, P. J. *J. Chem. Phys.* **1985**, *82*, 284.

(9) (a) Dunning, T. M., Jr. *J. Chem. Phys.* **1971**, *55*, 716. (b) Dunning, T. M., Jr. *J. Chem. Phys.* **1970**, *53*, 2823.

(10) Binkley, J. S.; Pople, J. A.; Hehre, W. J. Self-Consistent Molecular Orbital Methods. 21. *J. Am. Chem. Soc.* **1980**, *102*, 939.

(11) Ehlers, A. W.; Böhme, M.; Dapprich, S.; Gobbi, A.; Höllwarth, A.; Jonas, V.; Köhler, K. F.; Stegmann, R.; Veldkamp, A.; Frenking, G. *Chem. Phys. Lett.* **1993**, *208*, 111.

(12) Fresch, M. J.; Trucks, G. W.; Schlegel, H. B.; Gill, P. M. W.; Johnson, B. G.; Robb, M. A.; Cheesemen, J. R.; Keith, T. A.; Petersson, J. A.; Montgomery, J. A.; Raghavachari, K.; Al-Laham, M. A.; Zakrzewski, V. G.; Ortiz, J. V.; Foresman, J. B.; Cioslowski, J.; Stefanov, B. B.; Nanayakkara, A.; Challacombe, M.; Peng, C. Y.; Ayala, P. Y.; Chen, W.; Wong, M. W.; Andres, J. L.; Replogle, E. S.; Gomperts, R.; Martin, R. L.; Fox, D. J.; Binkley, J. S.; DeFrees, D. J.; Baker, J.; Stewart, J. J. P.; Head-Gordon, M.; Gonzales, C.; Pople, J. A. Gaussian 94; Gaussian Inc., Pittsburgh, PA, 1995.

(13) Cui, Q.; Musaev, D. G.; Svensson, M.; Morokuma, K. *J. Phys. Chem.* **1996**, *100*, 10936.

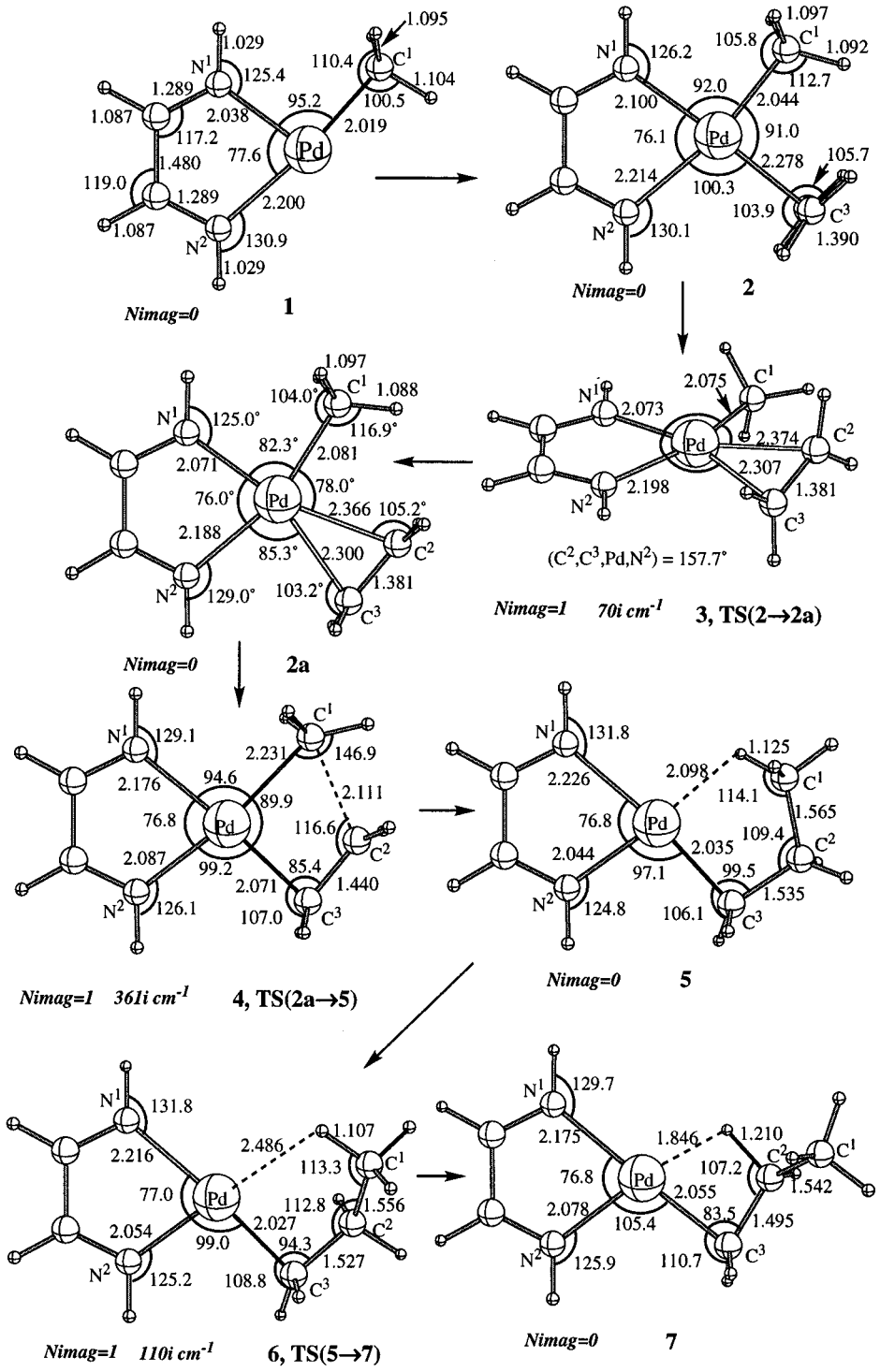

Figure 1. Calculated bond distances (in Å) and angles (in deg) of the reactants, transition states, intermediates, and products of the initiation reaction (1): $[L_2PdCH_3]^+ + C_2H_4 \rightarrow [L_2PdCH_2CH_2CH_3]^+$.

The next step of the reaction is the coordination of olefin to complex **1**, which may lead to two different π-complexes, **2** and **2a**, where the olefin is positioned perpendicular or planar to the $N^1PdN^2C^1$ plane, respectively. Both of these structures were positively characterized to be real minima. The addition of olefin slightly changes the geometries from complex **1**, with the exception of the Pd−N^1 bond distance, positioned trans to the coordinating olefin, which is elongated by 0.1 Å. The geometry of complex **2a** is slightly different from **2**, with significant differences seen in the Pd−olefin bonds: in **2** the Pd−C^2 and Pd−C^3 bonds are equal, 2.278 Å, while in **2a** the Pd−C^2 bond is 0.066 Å longer than Pd−C^3.

Complex **2** is 4.6 kcal/mol lower in energy than **2a** and is separated from it with a barrier of 5.0 kcal/mol at transition state **3**. The structure **3** is a real transition state with one imaginary frequency of *70i* cm^{-1} corresponding to the rotation of C_2H_4 around the Pd−X axis, X being the center of the $H_2C{=}CH_2$ bond. The Gibbs free energies for the difference between the structures **2** and **2a** and for the barrier separating **2** from **2a** are 3.4 and 6.2 kcal/mol, respectively. The complexion energy of **1** + C_2H_4 is calculated to be 33.9 and 31.5 kcal/

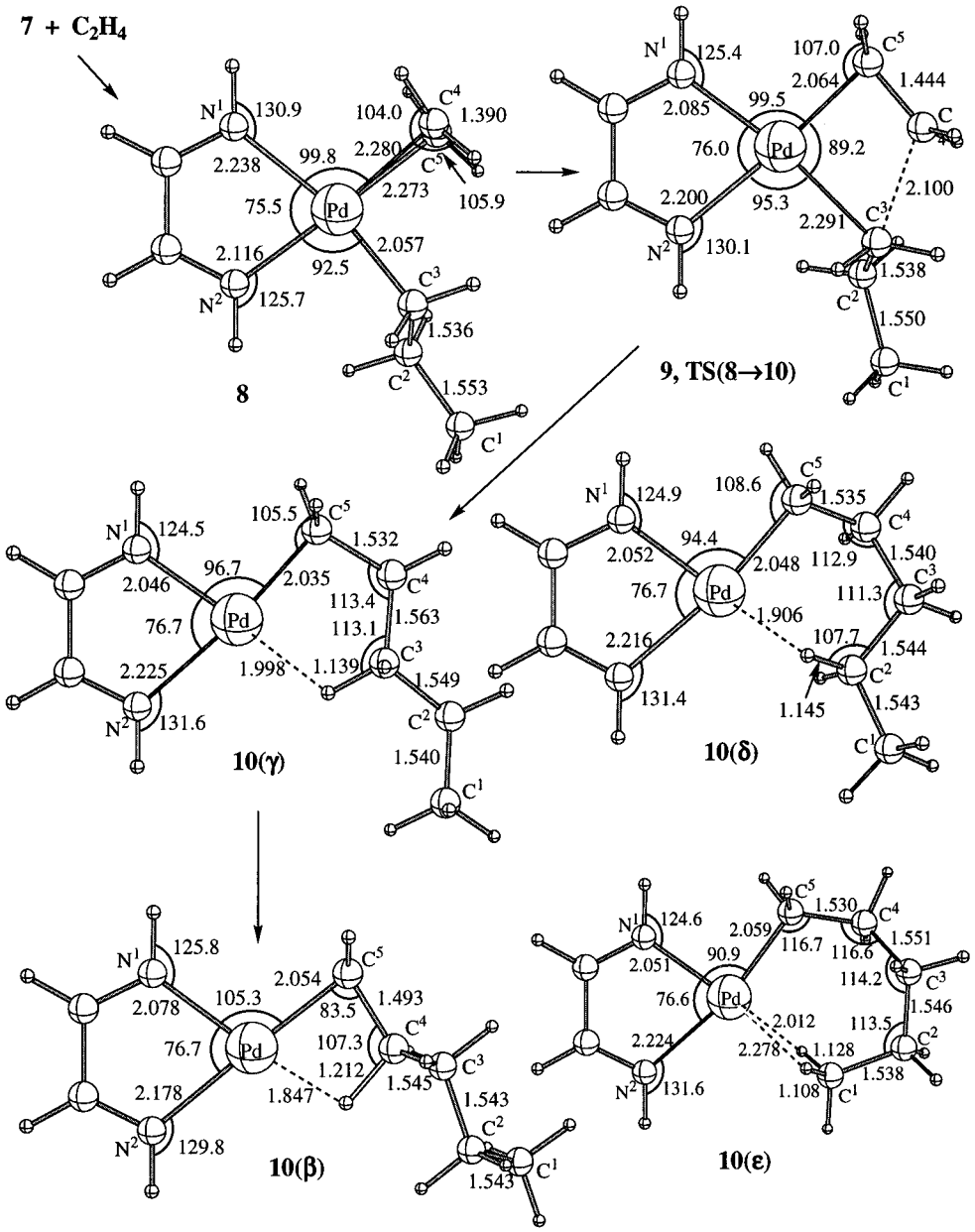

Figure 2. Calculated bond distances (in Å) and angles (in deg) of the transition states, intermediates, and products of the propagation (olefin coordination and insertion for linear polymer) reaction (2), $[L_2PdCH_2CH_2CH_3]^+ + C_2H_4 \rightarrow [L_2Pd(CH_2CH_2)_2CH_3]^+$.

mol without and with ZPC, respectively, which is reduced to 20.1 kcal/mol in the Gibbs free energy, as is expected from the entropy contribution. Since the transition state **3** corresponding to a rotation of olefin around the Pd−X axis is only 0.7 kcal/mol (with ZPC) or 2.8 kcal/mol (using the Gibbs free energy) higher than complex **2a**, one can conclude that complex **2a** easily rearranges to complex **2**. With a high barrier for further conversion (vide infra), diimine π-alkene (σ-methyl) complex **2** is the initial resting stage of the active catalyst in the polymerization mixture.

From complex **2**, the reaction proceeds via transition state **4** (**TS(2a→5)**) which leads to the γ-agostic complex **5**. The transition state-structure **4** (**TS(2a→5)**) was confirmed to have only one imaginary frequency of *361i* cm^{-1}, while all frequencies of the γ-agostic complex **5** are real. During this olefin insertion process, the Pd−C^1 and Pd−C^2 bonds are broken and the Pd−C^3 and C^1−C^2 bonds are formed. Structure **5** is a real agostic complex with a Pd−$H^{agostic}$ bond distance of 2.10 Å and C−$H^{agostic}$ bond distance of 1.13 Å (vs 1.089 Å in the free C_2H_4 molecule), where the Pd−N^1 bond is longer by 0.13 Å while the Pd−N^2 is shorter by 0.17 Å compared with those in the reactant **2**. These changes once again can easily be explained in terms of the *trans* influence. As seen in Table 1, the insertion barriers with ZPC from **2** and **2a**, respectively, are 16.6 kcal/mol (16.7 kcal/mol using the Gibbs free energy) and 11.7 kcal/mol (13.6 kcal/mol). The direct product of the reaction, the γ-agostic complex **5**, is calculated to be 29.9 (with ZPC) and 18.1 kcal/mol (the Gibbs free energy) lower in energy than the reactants, **1** + C_2H_4. However, complex **5** can easily rotate around the C^2−C^3 bond, with a 2.2 (with ZPC) and 2.4 kcal/mol (the Gibbs free energy) rotational barrier at the transition state **6** (**TS(5→7)**) and give the more stable β-agostic product **7**. The calculated energy difference, 8.1 kcal/mol with ZPC (8.5 kcal/mol using the Gibbs free energy) between the γ- and β-agostic products is consistent with the geometry changes shown in Figure 1. First, the Pd−$H^{agostic}$ bond

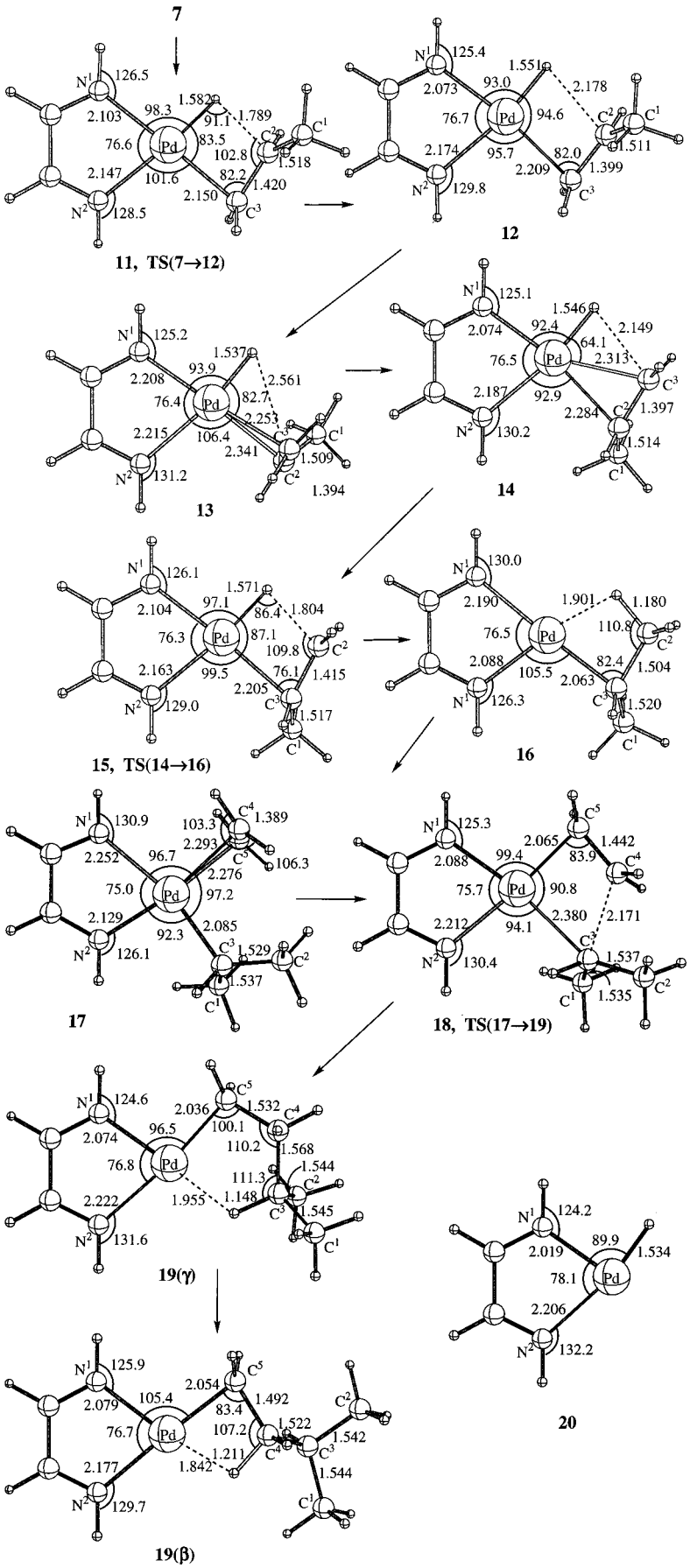

Figure 3. Calculated bond distances (in Å) and angles (in deg) of the transition states, intermediates, and products of the propagation (β-hydride elimination and olefin reinsertion for branched polymer) reactions (path **B**) (a) $[L_2PdCH_2CH_2\text{-}CH_3]^+ \rightarrow [L_2Pd(H)(CH_2{=}CHCH_3)]^+ \rightarrow [L_2PdCH(CH_3)_2]^+$ and (b) $[L_2PdCH(CH_3)_2]^+ + C_2H_4 \rightarrow [L_2Pd(CH_2CH_2)CH(CH_3)_2]^+$, as well as the complex L_2PdH^+ (**20**).

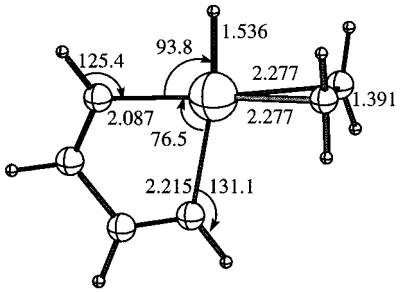

21

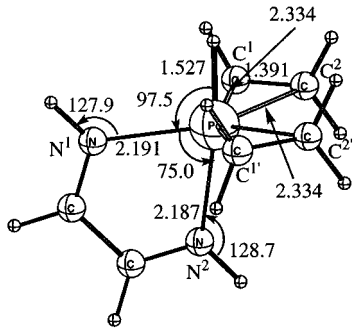

Nimag=0 **22**

Figure 4. Calculated bond distances (in Å) and angles (in deg) of the diimine−PdH(C_2H_4) (**21**) and five-coordinated bis(ethylene) complex **22** in C_s symmetry.

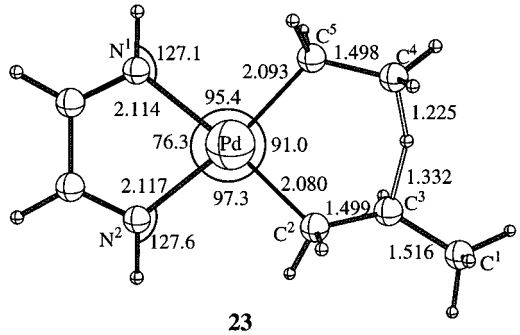

23

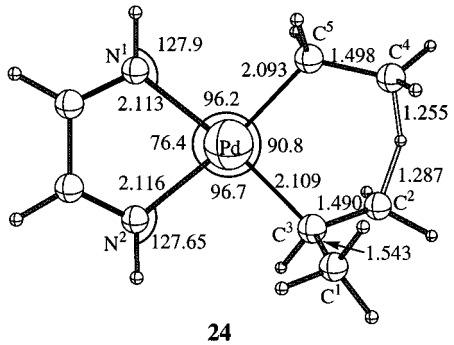

24

Figure 5. Calculated bond distances (in Å) and angles (in deg) of the molecular complexes and transition states of the hydrogenolysis reaction (4), $[L_2PdR]^+ + H_2 \rightarrow [L_2Pd(H_2)R]^+ \rightarrow [L_2PdH]^+ + HR$, where R = CH_3, C_2H_5, and C_3H_7.

in **7** (1.85 Å) is 0.25 Å shorter than that in **5** (2.10 Å). Consequently, the Pd−N^2 bond positioned *trans* to the agostic hydrogen is 0.04 Å longer in the β-agostic complex **7** than in the γ-agostic complex **5**. Second, the $C-H^{\beta-agostic}$ bond (1.21 Å) is 0.09 Å longer than the $C-H^{\gamma-agostic}$ one (1.12 Å).

Thus, the entire reaction (1) is calculated to be 38.0 kcal/mol exothermic with ZPC (26.6 kcal/mol using the Gibbs free energy), and the rate-determining step is the insertion of olefin into the Pd−alkyl bond, which takes place with a barrier of 16.6 kcal/mol with ZPC (16.7 using the Gibbs free energy). Note that the Gibbs free energy barrier for migratory insertion, 16.7 kcal/mol, is in excellent agreement with the experimental value, 17.2 kcal/mol.[3]

B. Chain Propagation. In all the subsequent sections, we did not perform normal-coordinate analysis. Thus, all the energies are without ZPC. The β-agostic intermediate **7** is a key intermediate on the PEP of the entire polymerization reaction. From this complex the reaction will split into several paths.

Path A: Olefin Coordination and Insertion for Linear Polymer. The initial step of path **A**, reaction 2, is the addition of an olefin molecule to the β-agostic intermediate **7**. In general, there are two different reaction paths: (1) frontside coordination of olefin to **7**, followed by a rotation of the alkyl group around Pd−C_α, and insertion of the olefin into the Pd−C_α bond, and (2) backside coordination of olefin to **7** and then insertion into the Pd−C_α bond. However, a preliminary study shows that the backside insertion path is highly unfavorable and, therefore, we did not study it. The frontside coordination of olefin to **7** leads to the new alkyl olefin complex **8**, calculated to be 58.6 and 17.1 kcal/mol exothermic relative to the **1** + 2 C_2H_4 and **7** + C_2H_4 dissociation limits, respectively. Comparison of the complexation energy, 17.1 kcal/mol, of **7** + C_2H_4 with 33.9 kcal/mol for **1** + C_2H_4 shows that the olefin binds 16.8 kcal/mol more weakly to complex **7** than to **1**. This can be understood by analyzing the geometries of the reactants, **1** and **7**, and complexes, **2** and **8**, respectively. As seen in Figures 1 and 2, the coordination of olefin to **1** is not accompanied by substantial geometry changes, while the coordination to **7** deforms the geometry of the reactant. As a result, its β-agostic feature disappears in **8** and lowers the stabilization energy. An analogy with the initialization step which had **2** and **2a** suggests that there may exist a structure **8a** with an in-plane olefin. Since its role in the reaction mechanism is not important, we have not searched for such a structure. With a high barrier for further conversion (vide infra), the diimine π-alkene σ-alkyl complex **8** is a resting stage of the catalyst with a growing polymer in the polymerization mixture.

The next step of the reaction (2) is the migratory insertion of olefin into the Pd−$CH_2CH_2CH_3$ bond via the transition state **TS(8→10)** (**9**) to give a new metal−alkyl complex, $L_2PdC_5H_{11}^+$ (**10**). As seen in Figures 1 and 2, the structures of the transition states **9** and **4**, which are for olefin insertion into the Pd−CH_3 and Pd−CH_2-CH_2CH_3 bonds, respectively, are very similar. **9** is an early transition state with its geometry close to that of the reactant **8**, but in comparison with **4**, it is slightly later. The barrier height calculated relative to complex **8** is 17.5 kcal/mol vs 16.3 kcal/mol for the chain initiation reaction (1). After the transition state is crossed, reaction (2) gives the product $L_2PdC_5H_{11}^+$ (**10**). In general, for the $L_2PdC_5H_{11}^+$ complex several structures with α-, β-, γ-, δ-, and ϵ-agostic hydrogens may exist. The calculations carried out without symmetry

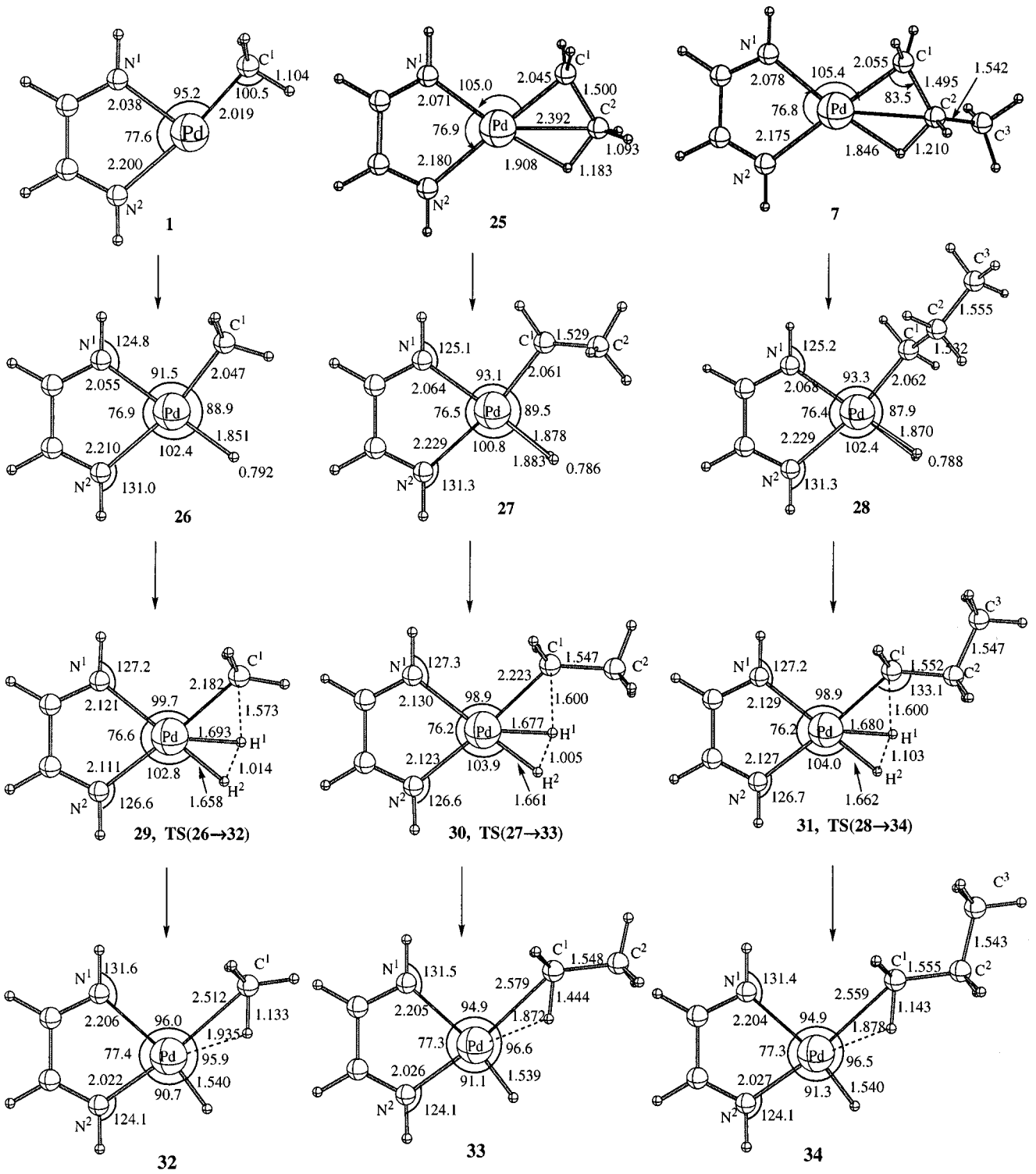

Figure 6. Calculated bond distances (in Å) and angles (in deg) of the transition states of the hydrogen exchange process between olefin and alkyl fragments of the complex $[L_2Pd(R)C_2H_4]^+$, where R = *n*-C_3H_7 and *i*-C_3H_7.

constraint located only the structures **10(*β*)**, **10(*γ*)**, **10-(*δ*)**, and **10(*ϵ*)** with *β*-, *γ*-, *δ*-, and *ϵ*-agostic hydrogens, respectively. A structure corresponding to the α-agostic complex converges with essentially no barrier into *β*- or *δ*-agostic complexes, depending on the initial guess in the geometry optimization. The *β*-agostic structure is calculated to be energetically lower than *γ*-, *δ*-, and *ϵ*-agostic complexes by 6.1, 1.7, and 3.8 kcal/mol, respectively. The trend in the relative stability of the *β*-, *γ*-, *δ*-, and *ϵ*-agostic complexes, $\beta > \delta > \epsilon > \gamma$, is in good agreement with the trend in the Pd−$H^{agostic}$ bond lengths, *β* (1.847 Å) < *δ* (1.906 Å) < *ϵ* (1.991 Å) < *γ* (1.998 Å), and (with some exceptions) with the C−$H^{agostic}$ bond lengths, *β* (1.212 Å) < *δ* (1.145 Å) < *γ* (1.139 Å) < *ϵ* (1.128 Å). The direct product, **10(*γ*)**, is expected to rearrange easily to the more stable **10(*β*)**.

These findings agree well with the conclusions of previous studies; the most stable conformation of the polymer chain contains a *β*-agostic interaction.[2cd,14−16]

(14) Alameddin, N. G.; Ryan, M. F.; Eyler, J. R.; Siedle, A. R.; Richardson, D. E. *Organometallics* **1995**, *14*, 5005 and references therein.

Table 1. Relative Energies (kcal/mol) of the Reactions (1)−(5) Calculated at the B3LYP Level using Different Basis Sets

	structure	ΔE_{rel}(BSI)	ΔE_{rel}(BSII)
Chain Initiation: Reaction 1			
$[L_2PdMe]^+ + C_2H_4$	**1**	0.0[a]	0.0[b]
$[L_2PdMeC_2H_4]^+$	**2**	−31.7/−29.3//−17.9[c]	−33.9/−31.5//−20.1
$[L_2PdMeC_2H_4]^+$	**3 (TS(2→2a))**	−26.6/−24.0//−11.6	−28.9/−26.3//−13.9
$[L_2PdMeC_2H_4]^+$	**2a**	−26.8/−24.1//−14.2	−29.3/−26.6//−16.7
$[L_2PdMeC_2H_4]^+$	**4 (TS(2a→5))**	−15.5/−12.8//−1.3	−17.6/−14.9//−3.4
$[L_2Pd(n\text{-}C_3H_7)]_\gamma^+$	**5**	−31.8/−27.8//−16.0	−33.9/−29.9//−18.1
$[L_2Pd(n\text{-}C_3H_7)]_\gamma^+$	**6 (TS(5→7))**	−29.7/−26.2//−14.2	−31.2/−27.7//−15.7
$[L_2Pd(n\text{-}C_3H_7)]_\beta^+$	**7**	−37.4/−33.9//−22.5	−41.5/−38.0//−26.6
Chain Propagation (Linear Polymer, Path A): Reaction 2			
$[L_2Pd(n\text{-}C_3H_7)]_\beta^+ + C_2H_4$	**7**	−37.4 (0.0)	−41.5 (0.0)
$[L_2Pd(n\text{-}C_3H_7)C_2H_4]^+$	**8**	−55.4 (−18.0)[d]	−58.6 (−17.1)
$[L_2Pd(n\text{-}C_3H_7)C_2H_4]^+$	**9 (TS(8→10))**	−38.1 (−0.7)	−41.1 (0.4)
$[L_2Pd(n\text{-}C_5H_{11})_\beta]^+$	**10(*β*)**	−61.1 (−23.7)	−66.7 (−24.5)
$[L_2Pd(n\text{-}C_5H_{11})_\gamma]^+$	**10(*γ*)**	−56.3 (−18.9)	−60.5 (−19.0)
$[L_2Pd(n\text{-}C_5H_{11})_\delta]^+$	**10(*δ*)**	−60.8 (−23.4)	−65.0 (−23.5)
$[L_2Pd(n\text{-}C_5H_{11})_\epsilon]^+$	**10(*ε*)**	−58.5 (−21.1)	−62.9 (−21.4)
Chain Propagation (*β*-Hydride Elimination and Olefin Reinsertion for Branched Polymer, Path B): Reaction 3			
$[L_2Pd(n\text{-}C_3H_7)]_\beta^+ + C_2H_4$	**7**	−37.4 (0.0)	−41.5 (0.0)
$[L_2Pd(n\text{-}C_3H_7)_\beta]^+ + C_2H_4$	**11 (TS(7→12))**	−31.5 (5.9)	−36.3 (5.2)
$[L_2PdH(C_3H_6)]^+ + C_2H_4$	**12**	−32.0 (5.4)	−36.5 (5.0)
$[L_2PdH(C_3H_6)]^+ + C_2H_4$	**13**	−31.7 (5.7)	−35.9 (0.4)
$[L_2PdH(C_3H_6)]^+ + C_2H_4$	**14**	−31.9 (5.5)	−36.4 (5.1)
$[L_2PdH(C_3H_6)]^+ + C_2H_4$	**15 (TS(14→16))**	−30.8 (6.6)	−35.7 (5.8)
$[L_2Pd(i\text{-}C_3H_7)]^+ + C_2H_4$	**16**	−39.4 (−2.0)	−42.6 (−1.1)
$[L_2Pd(i\text{-}C_3H_7)C_2H_4]^+$	**17**	−53.6 (−16.2)	−56.4 (−14.9)
$[L_2Pd(i\text{-}C_3H_7)C_2H_4]^+$	**18 (TS(17→19))**	−36.1 (1.3)	−38.9 (2.6)
$[L_2Pd(i\text{-}C_5H_{11})_\beta]^+$	**19(*β*)**	−61.7 (−24.3)	−67.3 (−25.8)
$[L_2Pd(i\text{-}C_5H_{11})_\gamma]^+$	**19(*γ*)**	−56.2 (−18.8)	−60.1 (−18.6)
Chain Termination (*β*-Hydride Elimination and Dissociation): Reaction 4			
$[L_2PdH(C_3H_6)]^+$	**12**	−32.0 (5.4)	−36.5 (5.0)
$[L_2PdH]^+ + CH_2{=}CHCH_3$	**20**	9.9 (41.9)	7.4 (43.9)
Chain Termination (*β*-Hydride Elimination and Associative Displacement): Path C			
$[L_2PdH]^+ + 2\ C_2H_4$	**20**	0.0	0.0
$[L_2PdH(C_2H_4)]^+ + C_2H_4$	**21**	−38.1	−39.9
$[L_2PdH(C_2H_4)(C_2H_4)]^+$	**22**	−43.2	
Chain Termination (Hydrogen Exchange)			
$[L_2Pd(n\text{-}C_3H_7)C_2H_4]^+$	**8**	−55.4 (−18.0)[d]	−58.6 (−17.1)
$[L_2Pd(n\text{-}C_3H_7)(C_2H_4)]^+$	**23 (TS(8→))**	−12.7	−18.0
$[L_2Pd(i\text{-}C_3H_7)C_2H_4]^+$	**17**	−53.6 (−16.2)	−56.4 (−14.9)
$[L_2Pd(i\text{-}C_3H_7)(C_2H_4)]^+$	**24 (TS(17→))**	−4.9	
Chain Termination (Hydrogenolysis): Reaction 5			
$[L_2PdMe]^+ + H_2 + C_2H_4$	**1**	0.0[a]	0.0[b]
$[L_2Pd(CH_3)(H_2)]^+ + C_2H_4$	**26**	−13.3	−16.8
$[L_2Pd(CH_3)HH]^+ + C_2H_4$	**29 (TS(26→32))**	−3.8	−10.4
$[L_2PdH(CH_4)]^+ + C_2H_4$	**32**	−22.4	−25.3
$[L_2PdH]^+ + CH_4 + C_2H_4$		−8.8	−10.1
$[L_2Pd(n\text{-}C_3H_7)]_\beta^+ + H_2$	**7**	−37.4 {0.0}	−41.5 {0.0}
$[L_2Pd(n\text{-}C_3H_7)(H_2)]^+$	**27**	−38.1 {−0.7}[e]	−42.5 {−1.0}
$[L_2Pd(n\text{-}C_3H_7)HH]^+$	**30 (TS(30→33))**	−26.9 {10.5}	−34.3 {7.2}
$[L_2PdH(C_3H_8)]^+$	**33**	−46.3 {−8.9}	−51.0 {−9.5}
$[L_2PdH]^+ + C_3H_8$		−29.5 {8.0}	−32.3 {9.2}
$[[L_2Pd(C_2H_5)]^+ + H_2$	**25**	[0][f]	[0]
$L_2Pd(C_2H_5)(H_2)]^+$	**28**	[−1.6]	[−2.1]
$[L_2Pd(C_2H_5)HH]^+$	**31 (TS(28→34))**	[9.8]	[6.0]
$[L_2PdH(C_2H_6)]^+$	**34**	[−9.9]	[−10.8]
$[L_2PdH]^+ + C_2H_6$		[6.0]	[6.9]

[a] Total energy is −551.160 02 au at the B3LYP/BSI level of theory. [b] Total energy is −552.229 70 au at the B3LYP/BSII level of theory. [c] Numbers after the single slant include the zero-point correction, while those after the double slants are the Gibbs free energies. [d] Numbers in parentheses are relative to the *β*-agostic complex **7**, without ZPC. [e] Numbers in braces are relative to $[L_2Pd(n\text{-}C_3H_7)] + H_2$. [f] Numbers in brackets are relative to $[L_2PdC_2H_5] + H_2$.

For example, Lohrenz et al.[17] have recently shown that for the butylbis(cyclopentadienyl)zirconium cation, $Cp_2Zr(CH_2CH_2CH_2CH_3)^+$, the most stable conformation is the *β*-agostic complex, and the α-, *δ*-, and *γ*-agostic structures are 11.2, 7.4, and 6.4 kcal/mol higher, respectively. The reactions **1** + 2 C_2H_4 → **10(*β*)** and **7** + C_2H_4 → **10(*β*)** are calculated to be exothermic by 66.7 and 25.2 kcal/mol, respectively.

Path B: *β*-Hydride Elimination and Olefin Reinsertion, Forming Branched Polymers. Path **B** starts from **7** with *β*-hydride elimination via transition state **11** and leads to the olefin hydride complex **12**.

(15) Weiss, H.; Ehrig, M.; Ahlrichs, R. *J. Am. Chem. Soc.* **1994**, *116*, 4919.
(16) Fan, L.; Harrison, D.; Deng, L.; Woo, T. K.; Swerhone, D.; Ziegler, T. *Can. J. Chem.* **1995**, *73*, 989.
(17) (a) Lohrenz, J. C. W.; Woo, T. K.; Fan, L.; Ziegler, T. *J. Organomet. Chem.* **1995**, *497*, 91. (b) Lohrenz, J. C. W.; Woo, T. K.; Ziegler, T. *J. Am. Chem. Soc.* **1995**, *117*, 12793.

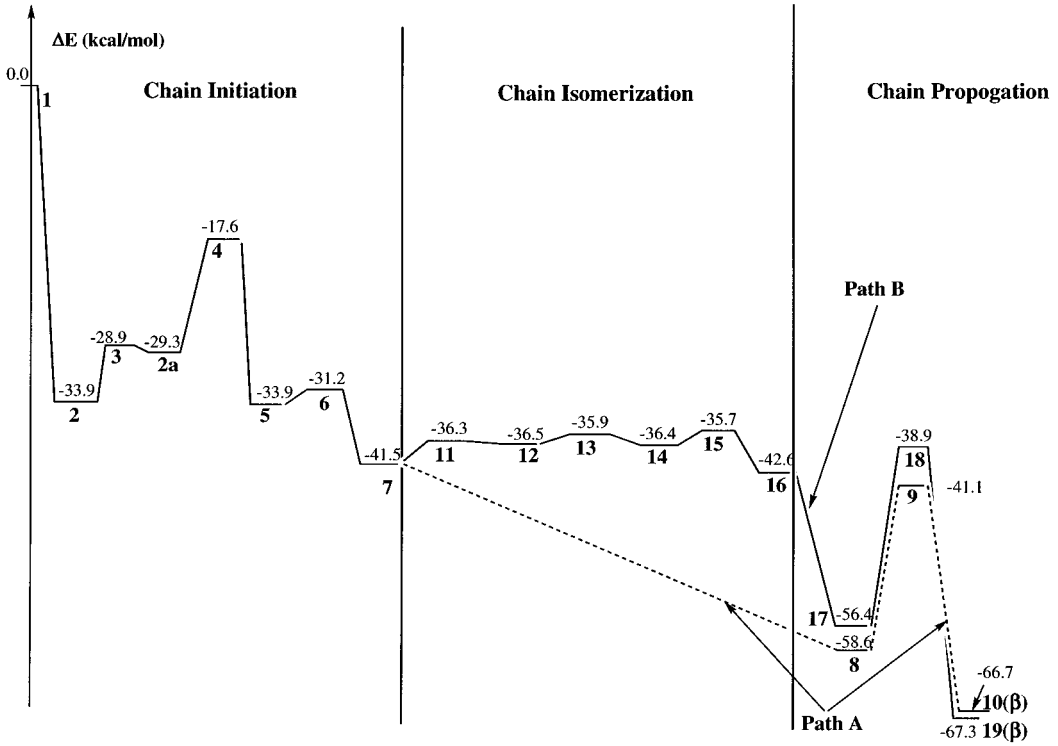

Figure 7. Potential energy profile of the $[L_2PdCH_3]^+$-catalyzed ethylene polymerization reaction. The relative energies are in kcal/mol, without ZPC.

Table 2. Binding Energies (in kcal/mol) of Important Bonds Related to the Reactions (1)−(5) Calculated at the B3LYP Level using Different Basis Sets

	structure	D_e(BSI)	D_e(BSII)
	σ Bonds		
$[L_2Pd]^+-H$	**20**	51.9	56.2
$[L_2Pd]^+-Me$	**1**	44.1	45.9
$[L_2Pd]^+-Et$		54.3	58.5
$[L_2Pd]^+-(n\text{-}C_3H_7)^a$	**7**	56.6	61.2
$[L_2Pd]^+-(i\text{-}C_3H_7)^a$	**16**	54.5	58.5
$[L_2Pd]^+-(n\text{-}C_5H_{11})$	**10(*β*)**	58.0	62.4
$[L_2Pd]^+-(i\text{-}C_5H_{11})$	**19(*β*)**	58.1	62.6
	π Bonds		
$[L_2PdH]^+-C_2H_4$		38.1	39.9
$[L_2PdH]^+-C_3H_6$	**12**	41.9	43.9
$[L_2PdMe]^+-C_2H_4$	**2**	31.7	33.9
$[L_2PdEt]^+-C_2H_4$		19.3	18.8
$[L_2Pd(n\text{-}C_3H_7)_\beta]^+-C_2H_4$	**8**	18.0	17.2
$[L_2Pd(i\text{-}C_3H_7)_\beta]^+-C_2H_4$	**17**	14.2	13.8

[a] $CH_3 + C_2H_4 \rightarrow$ 1-propyl + 24.9 (26.2) kcal/mol and $CH_3 + C_2H_4 \rightarrow$ 2-propyl + 28.9 (30.1) kcal/mol at the B3LYP/BSI (BSII) level.

Then, reinsertion with opposite regiochemistry occurs, leading to a branched polyethylene product. As was mentioned above, for the *β*-agostic product **7** the $C-H^{a\text{-}}_{gostic}$ bond length is calculated to be 0.12 Å longer than a nonagostic C−H bond. Therefore, one may expect that the *β*-hydride elimination will proceed with a small barrier. Indeed, as shown in Table 1, activation of the $C-H^{agostic}$ bond takes place with a 5.2 kcal/mol barrier relative to the *β*-agostic complex **7**. The transition state corresponding to this process, **TS(7→12)** (**11**), is a late transition state, as shown in Figure 3. The resultant complex, **12**, is an asymmetric olefin *π*-complex, which can easily rearrange both to the *β*-agostic product **7** and to more symmetric olefin *π*-complexes, **13** and **14**, structures optimized without symmetry constraint. The barrier height from **12** to **7** is calculated to be only 0.2 kcal/mol. The barriers separating **12** from **13** and **13** from **14** correspond to the rotation of the CH_2CHCH_3 fragment around the Pd−X axis, X being the center of the $CH_2{=}CHCH_3$ double bond. We did not locate these transition states. Probably they are less than 1 kcal/mol, as was found in the similar **2** → **2a** rearrangement. PEP for the rearrangement **11** → **12** → **13** → **14** is very flat, and the expected barriers and energy differences between the different isomers are less than 1 kcal/mol. Therefore, we will not discuss the energetics of **11**−**14** and the corresponding rotational transition states in detail, since this area of the PEP is not the rate-determining step of the entire reaction. The final *π*-complex **14** will reinsert the olefin with different regiochemistry to form the new Pd−alkyl complex **16** with a small barrier (0.8 kcal/mol) at the transition state **TS(12→16)** (**15**). As seen in Figure 3, **15** is an early transition state; its geometry and stability are very close to those for the reactant **14**. The resultant alkyl complex **16** is 6 kcal/mol more stable than the *π*-complexes **12** and **14**. On the basis of these results, one may conclude that *π*-complexes **12**−**14** are unlikely to exist under experimental conditions and the *β*-agostic intermediate **7** will rearrange with a barrier of 5−6 kcal/mol into the new alkyl complex **16**. The entire process **7** → **16** is calculated to be exothermic by 1 kcal/mol.

Next, the olefin coordinates to the alkyl complex **16**, to form the olefin alkyl complex **17**, in which olefin is arranged perpendicular to the $N^1PdN^2C^3$ plane. The structure with the olefin in plane does not exist and rearranges to **17** without a barrier. The calculated geometries of the $L_2Pd-C_2H_4$ fragment of **17** resemble those of **8**, while the calculated **16** + C_2H_4 complexation energy, 13.8 kcal/mol, is 3.4 kcal/mol smaller than that (17.1 kcal/mol) of **7** + C_2H_4. The exothermicity of the reaction **1** + 2 C_2H_4 → **17** is calculated to be 56.4 kcal/mol.

Scheme 1. Proposed Mechanism of the Pd(II)- and Ni(II)-Catalyzed Ethylene Polymerization Reaction

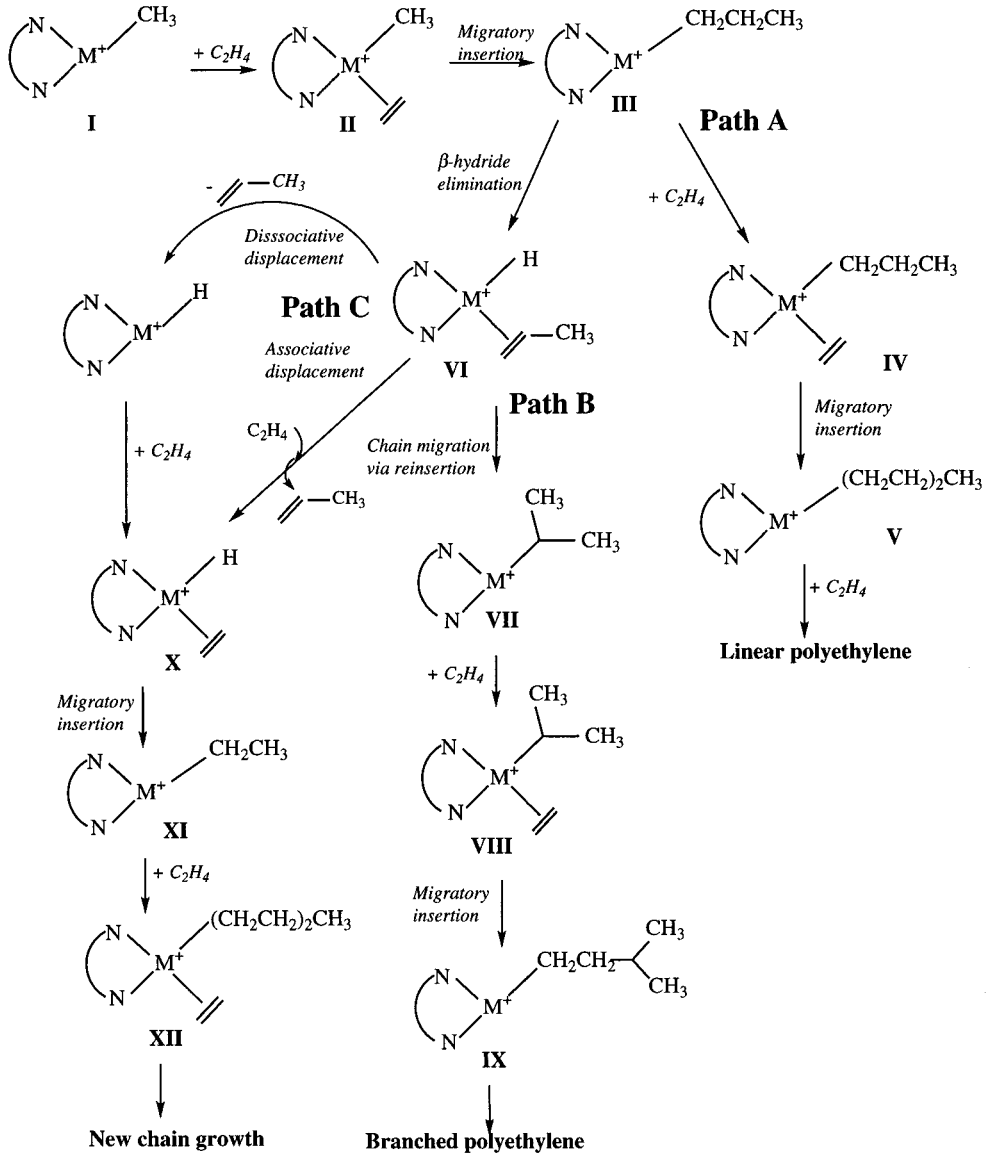

The following step of the reaction is the migratory insertion of olefin into the $L_2Pd-CHCH_3CH_3$ bond in **17**, which occurs through transition state **18** to give complex **19**. The insertion barrier is calculated to be 17.5 kcal/mol relative to the π-complex **17**. This is comparable to the barriers for olefin insertion into the L_2Pd-CH_3 bond in **2** and the $L_2Pd-CH_2CH_2CH_3$ bond in **8**, which are 16.3 and 17.5 kcal/mol, respectively. This is an early transition state, like **3** and **9**; its geometry is close to that of the reactant **17**. The product complex $[L_2Pd(CH_2CH_2)CH(CH_3)_2]^+$ (**19**) in general may also have several isomers with α-, β-, γ-, and δ-agostic hydrogens. As was shown above during the discussions of the structures and energetics of $[L_2PdC_5H_{11}]^+$ (**10**), among these different isomers the β-agostic structure is the global minimum and the complexes with γ-, δ-, and ϵ-agostic interactions are a few kcal/mol higher in energy. Therefore, for complex **19**, we only calculated the structures with the β- and γ-agostic interactions (**19-(*β*)** and **19(*γ*)**). As seen in Table 1, **19(*β*)** is 7.2 kcal/mol lower in energy than **19(*γ*)**. As seen in Figure 3, the $Pd-H^{agostic}$ bond distance increases via β(1.842 Å) < γ(1.955 Å), and the $C-H^{agostic}$ bond distance decreases via β(1.212 Å) < γ(1.148 Å), which correlates nicely with the energetics. Reactions **1** + 2 C_2H_4 → **19(*β*)**, **7** + C_2H_4 → **19(*β*)**, and **14** + C_2H_4 → **19(*β*)** are calculated to be exothermic by 67.3, 25.8, and 24.7 kcal/mol, respectively.

C. Chain Termination or Chain Transfer Processes. For metallocene-catalyzed olefin polymerization reactions several different kinds of chain termination processes have been reported:[1,2] β-hydride transfer, alkene C−H bond activation by metal−alkyl complexes, H exchange between alkyl and olefin fragments of the metal alkyl olefin complexes, and hydrogenolysis. In general, it was shown that hydrogenolysis, C−H bond activation, and H exchange are the most important chain-terminating processes for early transition elements.[2d,17b] Here, for the Pd(II)-catalyzed olefin polymerization reaction, we will briefly discuss the β-hydride transfer and H-exchange reaction and also study the hydrogenolysis reaction. In addition, we will discuss chain transfer via an *associative displacement* mechanism (path **C** in Scheme 1) reported by Brookhart and co-workers.[3] The C−H bond activation process for late

transition metals such as Ni, Pd, and Pt will be discussed in a separate paper due to the importance of this issue.[18]

***β*-Hydride Transfer and Dissociation.** The *β*-hydride transfer process has been discussed in detail in section B. For the Pd−propyl complex, it was found that *β*-hydride transfer takes place with a small activation barrier (5.2 kcal/mol) via the four-center transition state **11** and leads to the olefin hydride complex **12**. From **12**, the reaction may proceed either via path **B**, to give branched polyethylene products, or via elimination of propylene, which terminates the polymer growth and forms the diimine−palladium−hydride complex **20**. Elimination of propylene from **12** is calculated to be endothermic by 43.9 kcal/mol. This value is 4 kcal/mol larger than the calculated complexation energy for $[L_2PdH]^+ + C_2H_4$ (39.9 kcal/mol). Therefore, one can conclude that the large endothermicity of the elimination $[L_2Pd(H)(C_2H_4)_nCH_3]^+ \rightarrow [L_2PdH]^+ + (C_2H_4)_nCH_3$ makes it an improbable termination step of the polymerization. Path **B** starting from the same olefin hydrido complex **12** and having a small activation barrier is expected to be more favored over the termination via dissociative elimination.

***β*-Hydride Transfer and Associative Displacement.** According to Brookhart et al.,[3] for an olefin complex such as **12**, the coordinating olefin rapidly exchanges with ethylene from the solution by an *associative* mechanism (path **C** in Scheme 1). This suggests the existence of a stable five-coordinate bis(olefin) complex or the presence of a low-lying five-coordinate olefin exchange transition state. Considering $[L_2Pd(H)(C_2H_4)]^+$ (**21**) as a model for **12**, we have found a five-coordinated bis(ethylene) complex, **22**, shown in Figure 4, which is confirmed to be a local minimum (nimag = 0). Complex **22** has a trigonal-bipyramidal structure with two equivalent olefins in the equatorial plane and with the C_s symmetry plane defined by the N^1PdN^2 plane. The structure of **22**, compared with that of the mono(olefin) complex **21**, is very similar but is slightly looser in general; the equatorial Pd−N and Pd−C distances are slightly longer. The binding energy of the second ethylene is calculated to be only 5 kcal/mol at the B3LYP/BSI level, which is 33 kcal/mol less than that for the first ethylene coordination shown in Table 1. This 18e species is electronically saturated and sterically very crowded but still has a small positive binding energy. We have unsuccessfully searched for a transition state for coordination of the second olefin without symmetry constraint, suggesting that the second olefin coordination takes place without a barrier. These results are consistent with the experimental observations that the activation barrier is very low, if present at all, for this associative displacement step. As emphasized by Brookhart and co-workers,[3] bulky substituents on the auxiliary ligand may play an important role, prohibiting rapid olefin exchange and thereby the chain termination. The effect of these bulky groups could also be related directly to the stability of **22**. In a future study, we intend to investigate this problem in detail.

H Exchange. As shown in Table 2, the H-exchange process between the alkyl and olefin fragments on the metal alkyl olefin complexes **8** and **17** is found to be inefficient as a chain termination process due to very high activation barriers, 40.6 and 46.9 kcal/mol for *n*-Pr $\rightarrow C_2H_4$ and *i*-Pr $\rightarrow C_2H_4$ (where Pr = propyl) at the transition states **24** and **25**, respectively, relative to the corresponding alkyl olefin *π*-complexes. Their structures given in Figure 5 are multicenter transition states where the exchanged H atom is slightly closer to ethylene than the alkyl fragments. Note that the chain termination processes, especially the H-exchange process, have recently been discussed in detail for the HNi(acac) catalyst by Ziegler and co-workers.[19]

Hydrogenolysis. Another chain termination process is the hydrogenolysis reaction (5), which may occur in the presence of hydrogen gas pressure and proceeds (as shown in Figure 6) via (i) coordination of a hydrogen molecule to the metal center, giving a dihydrogen complex, (ii) activation of H−H and formation of C−H bonds, and (iii) elimination of alkane, resulting in a diimine−Pd−hydride complex. The initial step of the reaction, coordination of H_2 to L_2PdR^+ (**1**, **25**, and **7**) gives dihydrogen complexes **26**−**28**, for R = CH_3, C_2H_5, and C_3H_7, respectively. Their structures are similar, for instance with H−H and Pd−H distances of around 0.79 and 1.85−1.88 Å, respectively. As seen in Table 1, the coordination energy of H_2 is 16.8, 2.1, and 1.0 kcal/mol for R = CH_3, C_2H_5, and C_3H_7, respectively. These large differences in the calculated coordination energy of H_2 to the reactant L_2PdR^+ for R = CH_3, C_2H_5, and C_3H_7 can be understood by comparison of the geometries of the reactants **1**, **25**, and **7** and the dihydrogen complexes **26**−**28**, respectively. As seen in Figure 6, the structure **1** has no agostic interaction, while the structures **25** and **7** have a strong *β*-agostic interactions. Upon complexation the *β*-agostic interaction is completely lost for **27** and **28**, and it may better be considered to be formed from the nonagostic structure. The structures **25′** and **7′** (not shown), which are structures **27** and **28** with the H_2 molecule removed and are non-*β*-agostic, are calculated to be 13.7 and 15.3 kcal/mol less stable than the *β*-agostic structures **25** and **7**, respectively. Therefore, relative to the nonagostic structures **25′** and **7′**, the reaction $L_2PdR^+ + H_2 \rightarrow [L_2PdR](H_2)^+$ is calculated to be exothermic by 15.8 and 16.3 kcal/mol for R = C_2H_5 and C_3H_7, respectively, which are nearly comparable with 16.8 kcal/mol for R = CH_3.

The next step, the activation of the H−H bond and formation of the C−H bond, takes place through a four-center transition state, structures **29**−**31** for R = CH_3, C_2H_5, and C_3H_7, respectively, in Figure 6. These are metathesis transition states where the H−H bond is broken and the $C-H^1$ and $Pd-H^2$ bonds are formed simultaneously. The geometries of those are again similar for R = CH_3, C_2H_5, and C_3H_7: the H−H, $C-H^1$, and $Pd-H^2$ bonds are all around 1.00−1.01, 1.57−1.60, and 1.66−1.67 Å, respectively. The barrier heights calculated relative to the dihydrogen complexes **26**−**28** are 6.4, 8.1, and 8.2 kcal/mol, respectively. There may exist an alternative pathway corresponding to the oxidative addition of H−H to the Pd center followed by reductive elimination of alkane. However, according to our preliminary calculations[18] the transition state to the

(18) Svensson, M.; Musaev, D. G.; Morokuma, K. To be submitted for publication.

(19) (a) Fan, L.; Krzywicki, A.; Somogyvari, A.; Ziegler, T. *Inorg. Chem.* **1996**, *35*, 4003. (b) Fan, L.; Krzywicki, A.; Somogyvari, A.; Ziegler, T. *Stud. Surf. Sci. Catal.* **1996**, *100*, 507.

oxidative-addition path is energetically unfavorable and unlikely to participate. The possibility of the existence of different pathways, metathesis and oxidative addition, for a late-transition-metal complex will be discussed in a separate paper in more detail.[19] After the barrier is overcome, the reaction leads to the alkane molecular complexes **32**−**34** for R = CH_3, C_2H_5, and C_3H_7, respectively. In the next step, these complexes dissociate alkane (RH) and generate L_2PdH^+. This alkane dissociation step is calculated to be endothermic by 15.2, 17.7, and 18.7 kcal/mol for RH = CH_4, C_2H_6, and C_3H_8, respectively, and takes place without a reverse barrier. The hydrogenolysis reactions to $L_2PdR^+ + H_2 \rightarrow L_2PdH^+ + RH$ are calculated to be exothermic by 10.1 kcal/mol for R = CH_3 and endothermic by 6.9 and 9.2 kcal/mol for R = C_2H_5 and C_3H_7, respectively.

Comparison of Various Chain Transfer and Termination Processes. Comparison of β-hydride transfer + dissociation, β-hydride transfer + associative displacement, H exchange, and hydrogenolysis chain termination processes shows that the H-exchange process, which requires a large activation barrier, is unlikely to be an efficient chain transfer mechanism. The β-hydride transfer + dissociation mechanism is also highly endothermic (43.9 kcal/mol) to dissociate propylene from the metal−olefin−hydride complex **12**, producing the hydride complex $[L_2PdH]^+$ in the gas phase. Though in solution the solvation of **20** would make the overall process much less endothermic, unless dissociation and solvation can take place simultaneously as in the associative displacement, the energy requirement would still be large. For an experimentally used solvent such as CH_2Cl_2, where the solvent coordination is not as strong as for olefin, associative olefin/solvent replacement is unlikely to be an efficient chain transfer/termination process. Thus, the associative displacement mechanism (path **C** in Scheme 1) where the coordinated polymer olefin rapidly exchanges with ethylene from the solution via a five-coordinate intermediate is likely to be the most favorable chain transfer mechanism in this polymerization reaction.

D. Comparison of Different Mechanisms of the Pd(II)-Catalyzed Olefin Polymerization Reaction. As seen in Table 1 and Figure 7, where the energetics and the potential energy profile (PEP) of the diimine−Pd-catalyzed ethylene polymerization reaction is shown, the insertion of olefin into the Pd−alkyl bond is the rate-determining step of the entire reaction. The calculated insertion barrier is 16.3 kcal/mol in the polymer initiation step. It increases to 17.5 kcal/mol for subsequent insertion reactions, regardless of the path. The olefin alkyl complexes are found to be stable by 33.9, 17.1, and 13.8 kcal/mol relative to the olefin dissociation for the initiation reaction (1) and propagation reactions (2) and (3), respectively. Therefore, one may conclude that the olefin alkyl complexes are the resting states in the catalytic cycle, which is in agreement with the experimental findings. The calculated insertion barriers also agree well with experimentally measured insertion barriers of 17.2 kcal/mol for olefin initiation and 17.6 kcal/mol for subsequent insertion reactions.[3]

The passage of the insertion transition state leads to the β-agostic complex **7**. The entire reaction $L_2PdR^+ + C_2H_4 \rightarrow L_2Pd(CH_2CH_2R)^+$ is calculated to be exothermic by 41.5 kcal/mol for R = CH_3. The exothermicity of the subsequent polymer growth reactions (2) and (3) decreases to 25.2 and 25.8 kcal/mol, respectively. This difference in the exothermicity of the polymer initiation reaction (1), on one side, and the polymer growth reactions (2) and (3), on the other side, has been explained above in terms of the absence of a β-agostic interaction in the reactant of the former, $L_2PdCH_3^+$ (**1**).

The β-agostic complex **7** constitutes an important point of the PEP of the entire process. From this point the reaction splits into two different channels leading to linear (path **A**) or methyl-branched (path **B**) polymers. As discussed above, path **A** starts by a frontside attack of ethylene at the β-agostic complex **7** without barrier and with a 17.1 kcal/mol energy gain. The first step of path **B** is the activation of β-agostic C−H with a 5−6 kcal/mol barrier at the four-center transition state **11**, which leads to the olefin hydride species **12**. Complex **12** can after rotation and reinsertion rearrange into the next Pd−alkyl complex, **16**. The entire process **7** → **16** has a relatively flat potential energy profile. The resulting alkyl complex **16** has a vacant site and may bind the next coordinating olefin molecule, affording the new olefin alkyl complex **17**, with an energy lowering of 13.8 kcal/mol.

In an experimental observation, cationic (phenanthroline)methylpalladium affords in the presence of ethylene substantial amounts of propylene (NMR) and only a modest yield of oligomers higher than butenes.[20] Our calculations with cationic (ethanediimine)methylpalladium show that, with **7** as starting material, olefin coordination for linear chain growth takes places without barrier, while β-hydride elimination for chain transfer (associative displacement) and branched growth requires a small but positive activation energy; this may be considered as contradicting the above experimental observation. However, one has to recognize that olefin coordination is a bimolecular process and requires slow diffusion of ethylene in solution, while β-elimination is a unimolecular process independent of diffusion and may actually be faster. The stabilization by the dielectric solvent CH_2Cl_2 ($\epsilon = 9.1$) may also favor the unimolecular β-elimination.

Experiments also indicate that bulky substituents on nitrogen are needed for high-molecular-weight polymer.[3] Though the effects of bulky substituents are not easy to estimate at this stage, comparing among three processes from the key intermediate **7**, one would expect that steric effects disfavor the most the associative displacement process which has to go through a sterically congested bis(olefin) complex, such as **22**. This should result in less chain transfer and higher molecular weight, consistent with experiment. It is also expected that the branched growth path **B**, requiring rotation of polymeric olefin in an intermediate complex, would be more influenced by the steric effects than the linear growth path **A**, while the process from **7** to **8** (path **A**) will be more subject to the solvent effects than to **12** (path **B**). Thus, the linear/branched ratio would be determined by a delicate balance between the solvent and substituent effects. This will be studied in detail in a forthcoming paper.

(20) Strömberg, S.; Oksman, M.; Zhang, L.; Zetterberg, K. *Acta Chem. Scand.* **1995**, *49*, 689.

Conclusions

From the present research, the following conclusions can be drawn.

1. The first step of the diimine−Pd(II)-catalyzed ethylene polymerization reaction is the coordination of ethylene to a metal center with a complexation Gibbs free energy of 20.1 kcal/mol. The insertion of the olefin into the metal−alkyl bond takes place with a 16.7 kcal/mol Gibbs free energy barrier and leads to the formation of a γ-agostic product which, with a small barrier, rearranges to the more stable β-agostic product **7**.

From the β-agostic complex **7**, the reaction splits into two different channels leading to linear (path **A**) or methyl-branched (path **B**) polymers. For path **A**, the reaction (2) starts by a frontside attack of ethylene at the β-agostic complex **7**, followed by the insertion of ethylene into the $Pd^+-CH_2CH_2CH_3$ bond, leading to the linear polymer β-agostic-$[L_2Pd(CH_2CH_2)_2CH_3]^+$. The first step of path **B** is the activation of a β-agostic $C^{\beta}-H^{agostic}$ bond with a barrier of 5−6 kcal/mol, which leads to the olefin hydride species **12**. Complex **12**, after rotation and reinsertion, rearranges into the $[L_2Pd(CH(CH_3)_2)]^+$ complex **16**, which has a vacant site and may bind the next olefin, giving the new olefin alkyl complex **17**. The insertion of olefin into the $L_2Pd^+-CH(CH_3)_2$ bond leads to the methyl-branched polyethylene species β-agostic-$[L_2Pd(CH_2CH_2)(CH(CH_3)_2)]^+$.

2. The rate-determining step of the entire polymerization reaction is the insertion of olefin into the L_2Pd^+-alkyl bond. The Gibbs free energy barrier is 16.7 kcal/mol for the initiation and is not much different in both linear and branched chain growth reactions. The calculated insertion barriers are in good agreement with experimentally measured[3] insertion barriers of 17.2 kcal/mol for olefin initiation and 17.6 kcal/mol for subsequent insertion reactions.

3. Both paths, **A** and **B**, start from β-agostic complex **7** and are exothermic, by 14.9 and 17.1 kcal/mol, respectively. However, path **A** starts by coordination of the ethylene molecule to the metal center without an energetic barrier, but a diffusion-related barrier will exist under normal experimental conditions, while path **B** and associative displacement mechanisms start with the activation of the β-agostic C−H bond, which occurs with a small (5−6 kcal/mol) β-hydride activation barrier. Thus, one would expect that Pd(II)-catalyzed ethylene polymerization will produce more linear than methyl-branched polyethylenes in the gas phase than would be the case under normal experimental conditions. However, as discussed above, both the ratio of polymer growth/chain transfer (molecular weight of polymer) and the ratio of linear/branched growth would be influenced very much by both the substituent and the solvent effects.

4. The most stable conformation of the $[L_2PdC_5H_{11}]^+$ complex is the structure with a β-agostic interaction. Its conformations with γ-, δ-, and ϵ-agostic interactions are calculated to be 6.1, 1.7, and 3.8 kcal/mol higher than the β-agostic interaction, respectively.

5. Two chain transfer processes are possible from the olefin hydride species **12**. The elimination of propylene from **12** is highly endothermic and is not likely to be a favorable pathway. An associative displacement from **12** where the coordinating olefin rapidly exchanges with ethylene from the solution (path **C** in Scheme 1) is likely to be the preferred chain transfer pathway. The H-exchange process between alkyl and olefin fragments at the L_2Pd−alkyl−olefin complex is found to be an inefficient chain termination process.

6. The hydrogenolysis, reaction 5, is also a favorable chain termination process in the presence of the hydrogen gas pressure. The first step is the coordination of H_2 to the metal center, which is exothermic by 16.8, 2.1, and 1.0 kcal/mol for R = CH_3, C_2H_5, and C_3H_7, respectively. Then the activation of the H−H bond and the formation of the C−H bond takes place through a four-center transition state with 6.4, 8.1, and 8.2 kcal/mol energetic barriers for R = CH_3, C_2H_5, and C_3H_7, respectively. The final step of the reaction is elimination of an alkane molecule to give the diimine−palladium−hydride complex.

Acknowledgment. The use of the computational facilities and programs at the NCSA (University of Illinois at Urbana-Champaign) and the Emerson Center is acknowledged. The present research is in part supported by grants (Nos. CHE-9409020 and CHE96-27775) from the National Science Foundation. M.S. acknowledges a Postdoctoral Fellowship from the Swedish Natural Science Research Council.

Supporting Information Available: Tables of Cartesian coordinates of all optimized structures (9 pages). Ordering information is given on any current masthead page.

OM961033J